

FAILURE IN Fe-Ni-Cu-Mo SINTERED STEEL UNDER STATIC TENSILE LOADING

EVA DUDROVÁ^{1*}, MARGITA KABÁTOVÁ¹, MIRIAM KUPKOVÁ¹

Microscopic crack initiation and crack propagation processes have been studied in a sintered Fe-Ni-Cu-Mo alloyed steel during static tensile testing. As-sintered and heat-treated specimens with density of $\sim 7.15 \text{ g}\cdot\text{cm}^{-3}$ were pressed from Fe-4%Ni-1.5%Cu-0.5%Mo diffusion alloyed powder (Distaloy AE) with addition of 0.7 % graphite. The microstructure of both as-sintered and heat-treated materials was characterised. Static tensile tests were carried out on the specimens with polished and etched surface under a gradually increased loading. The microcrack initiation and propagation processes in as-sintered and heat-treated microstructure were analysed by light and scanning electron microscopy. The observations showed that failure mechanisms are strongly dependent on matrix microstructure and pores localisation.

Key words: failure, Fe-Ni-Cu-Mo sintered steel, microstructure, tensile testing, microcrack initiation and propagation

PORUŠOVANIE SPEKANEJ OCELE Fe-Ni-Cu-Mo PRI STATICKOM ŤAHOVOM NAMÁHANÍ

V práci sme študovali mikroskopické procesy iniciácie a šírenia trhlín v spekannej Fe-Ni-Cu-Mo oceli pri statickej ťahovej skúške. Spekané a tepelne spracované vzorky hustoty $\sim 7,15 \text{ g}\cdot\text{cm}^{-3}$ sme vylišovali z difúzne legovaného prášku Fe-4%Ni-1,5Cu-0,5%Mo (Distaloy AE) s prídavkom 0,7 % grafitu. Charakterizovali sme mikroštruktúru v spekanom a v tepelne spracovanom stave. Vzorky s vylešteným a leptaným povrchom sme podrobili statickej ťahovej skúške pri postupnom zvyšovaní zaťaženia. Iniciáciu a šírenie mikrotrhlín v spekannej a v tepelne spracovanej mikroštruktúre sme analyzovali optickou a rastrovacou elektrónovou mikroskopiou. Výsledky pozorovaní ukázali, že mechanizmy porušovania silne závisia od zloženia mikroštruktúry matrice a od distribúcie pórov.

1. Introduction

The processing technology of sintered steels cannot avoid the presence of specific microstructural discontinuities, such as pores, original particle surfaces, and

¹ Ústav materiálového výskumu SAV, Watsonova 47, 043 53 Košice, Slovak Republic

* corresponding author

interface boundaries. All of them influence microcrack evolution in sintered microstructure when mechanically loaded. Porosity, a specific feature in sintered steels, appears as an interconnected and/or isolated microstructural component. When the interconnected porosity is dominant (when the total porosity, P_T , exceeds 10 %), particle connections act as the critical failure sites. Isolated pores (at $P_T < 5-6$ %) act as microstructural discontinuities with the stress-strain localisation. The original particle surface areas can accelerate the cracking in porous microstructure due to the presence of small pores and oxides. Depending on alloying mode and processing conditions, the matrix microstructure of sintered steels exhibits homogeneous or heterogeneous character.

The effect of pores and matrix microstructure on mechanical properties of sintered iron and steels has been extensively investigated and well-documented, e.g. [1–16]. Special attention has to be paid to the stress-strain interactions of pores and matrix microstructure, e.g. [4, 5, 8, 12, 13, 15, 16]. The analysis of the data suggests, that the mechanical behaviour of porous microstructure under stress cannot be fully described only by porosity. Depending on pore geometry and matrix microstructure, the external load results either in the localised plastic flow or in the early microcrack initiation [8, 13, 16, 17]. The failure mode of individual microvolumes is determined by the local stress-strain behaviour [9, 13, 15, 18]. Pompe et al. [13] described the mechanical behaviour of a porous microstructure by the local strain-hardening ratio, σ_y/σ_c , where σ_y is the local yield stress, and σ_c is the local strength. In microvolumes with a strong strain-hardening capacity (when $\sigma_y/\sigma_c < 1$), the extensive microplastic flow develops, while a low strain-hardening capacity ($\sigma_y/\sigma_c \rightarrow 1$) results in a strong localisation of microplastic strain. Straffelini et al. [18] quantified the failure evolution in sintered steels by calculating the damage rate expressed as the variation of damage with the macroscopic plastic strain. They described three stages of failure evolution as follows. The first stage is characterised by a high damage rate (the plastic strain is highly localised around the pores), the second stage is related to the plastic strain propagation into the interior of particles, the third stage corresponds to the unstable final fracture.

Sintered materials based on Fe-Ni-Cu-Mo diffusion alloyed powders usually exhibit an inhomogeneous matrix microstructure. It consists of ferrite, pearlite, bainite, Ni-rich martensite, and austenite structures, all of them having their typical localisation. The existence of free internal surfaces in sintered microstructure, such as pores and/or particle connections, results in several specific failure mechanisms. For static tensile loading, the following characteristic failure modes can be considered. In a highly porous and sufficiently plastic matrix, the basic failure mechanism is the interparticle ductile fracture. Depending on the geometry of particle connections, the point, line or dimple ductile fracture facets are formed [11]. A distinct case of interparticle failure is the separation along the original particle surfaces without or with only minimal local plastic flow [7]. The presence of oxides along

the grain boundaries in particle connections results in an interparticle intergranular failure. Transparticle transgranular ductile failure of sintered microstructure occurs only in the case of a low-porous and high-plastic matrix. When transgranular cleavage fracture develops in sintered steels it has a transparticle character. In a highly porous microstructure it may transform into interparticle ductile failure [8]. Pores can accelerate crack propagation by reducing the effective cross-section and by their micronotch effect. However, pores blunting the crack tip can stop the crack propagation [13].

In the present investigations, the microscopic crack initiation sites and crack propagation behaviour were studied in Distaloy AE sintered and heat-treated specimens subjected to gradually increased static tensile stresses.

2. Experimental material and procedure

Standard “dog-bone” specimens for tensile tests (ISO 2740 Standard) with the density of $\sim 7.15 \text{ g}\cdot\text{cm}^{-3}$ were produced from Fe-4wt.%Ni-1.5wt.%Cu-0.5wt.%Mo diffusion alloyed powder (Distaloy AE, produced by Höganäs, Sweden [19]) with addition of 0.7 wt. % of natural graphite and 0.8 wt. % HW wax as a lubricant. Sintering was carried out at the temperature of 1120°C for 60 minutes in cracked ammonia with a dew point of -30°C in industrial furnace (EBNER). Both heating and cooling rates were $\sim 10^\circ\text{C}/\text{min}$. The mean carbon content in sintered specimens was 0.64 %. Some of the sintered specimens were heat-treated as follows: austenitization at 860°C (cracked ammonia) \rightarrow oil quenching (60°C) stress relieving at 160°C/15 minutes.

The tensile tests were performed at room temperature on TIRATEST 2300 testing machine in accordance with the ISO 2740 standard at a cross-head speed of 0.2 mm/min and an extensometer with a gauge length of 25 mm. The preferential crack initiation sites and crack propagation processes were observed using light and scanning electron microscopy (Tesla BS 340 with EDS microanalyser Link ISIS 300).

3. Results and discussion

The final microstructure of sintered Distaloy AE steel specimens depends on the distribution of carbon and alloying elements and their diffusion transport involved in the sintering process. The microstructure resulting from sintering at 1120°C (Fig. 1) includes fine and coarse pearlite, bainite, martensite, and nickel-rich austenite structures. The microstructural regions originating from the interior of the iron particles contain pearlite and, sometimes, a small amount of ferrite was detected ($\sim 5\%$ of the observed area). Pearlite and bainite areas are frequently surrounded by Ni- and Cu-rich ferrite layers with dispersed cementite. The fraction of pearlite and bainite is $\sim 60\%$ of the observed area. Martensite exists in the

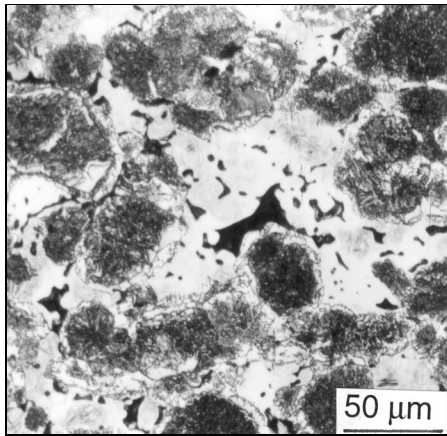


Fig. 1. Microstructure of the as-sintered Distaloy AE+0.7C steel.

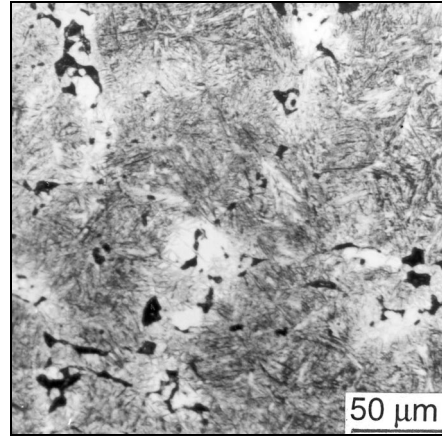


Fig. 2. Microstructure of the heat-treated Distaloy AE+0.7C steel.

Table 1. Composition range and microhardness of microstructural constituents of as-sintered Distaloy AE steel specimens

Microconstituents	Composition range [wt. %]	Microhardness HV 0.01
Ferrite		100–140
Pearlite	< 2.5 Ni; < 1.5 Cu	200–300
Bainite	~ 3 Ni; < 2.5 Cu; < 1 Mo	300–360
Martensite	4–11 Ni; ~ 3 Cu; ~ 1 Mo	450–600
Austenite	13–30 Ni; 5–8 Cu; ~ 1 Mo	150–200

regions through the nickel-rich austenite that is situated near the original particle surfaces. The area fraction of martensite and austenite structures is ~ 35 %. The microstructural constituents characterised by the chemical composition range and the microhardness HV 0.01 are listed in the Table 1. A step EDX microanalysis indicated that the nickel content in austenite is from 15 to 30 %, in martensite it drops to 4–11 %. Copper and molybdenum show similar quantitative distribution as nickel does.

The microstructure of heat-treated Distaloy AE sintered specimens (Fig. 2) consists of coarse martensite with the microhardness in the range of 550 to 880 HV 0.01 and by Ni-rich martensite and austenite regions (localised near pores) with the microhardness ranging from 200 to 400 HV 0.01. The area fraction of the Ni-rich martensite and austenite regions is about 30 %.

Table 2. Mechanical properties of as-sintered and heat-treated Distaloy AE steel

State	E [GPa]	$R_{p0.2}$ [MPa]	R_m [MPa]	A [%]	Hardness HV 30
As-sintered	143	366	603	1.2	246
Heat-treated	148	578	760	0.4	346

The static tensile properties and hardness of as-sintered and heat treated specimens are summarised in the Table 2. The true stress – true plastic strain curves for both the as-sintered and the heat-treated materials in Fig. 3a and Fig. 7a show continuous yielding of tested materials under tensile loading. Such behaviour of tested materials is connected with the heterogeneous microstress-strain distribution due to the interaction effect of pores and microstructural constituents.

In order to identify the preferential microcrack initiation sites and cracks propagation, the specimens with polished and etched surface were tested at gradually increased tensile stress. The observations were concentrated on the area where the specimen fracture was supposed to occur.

The chronology of the microcrack evolution under tensile loading of as-sintered specimens can be described as follows. The first microscopically identified microcracks appeared at a stress level of about 23 % of the material tensile strength. Their initiation is mostly connected with existing pores situated in the martensite regions (Fig. 3b). With increasing tensile stress a number of initiated microcracks increases. The micrographs in Figs. 3c–e show some examples of microcrack evolution at stress levels corresponding to ~ 60 % (c), ~ 80 % (d), ~ 90 % (e) of the specimen tensile strength. Microcrack propagation in martensite regions occurs by mixed mechanisms involving intergranular failure, transgranular cleavage and separation in structural discontinuities. However, the existence of a-priori transformation microcracks cannot be excluded. The branching of propagating cracks occurs frequently, while the original particle surfaces exhibit a linking effect in the cracks propagation path. The propagating cracks mostly follow the pore distribution, but in some cases the pores may stop the crack. At a tensile stress higher than ~ 80 % of the material strength, the majority of propagating cracks reaches the martensite-bainite or pearlite interface boundaries. At this moment the crack either stops (Fig. 4), or continues to propagate along the interface boundary (Fig. 5). The increase of the tensile stress close to the material tensile strength results in mutual microcracks joining, and several large cracks are formed. Some of them result in the formation of a main crack (Fig. 6).

The microcracks initiation sites in the heat-treated specimens are linked to the pores situated near the previous particle surfaces in the martensite regions. The first microcracks were identified at tensile stresses of about 30 % of the heat-treated material tensile strength. With increasing loading the microcracks are growing

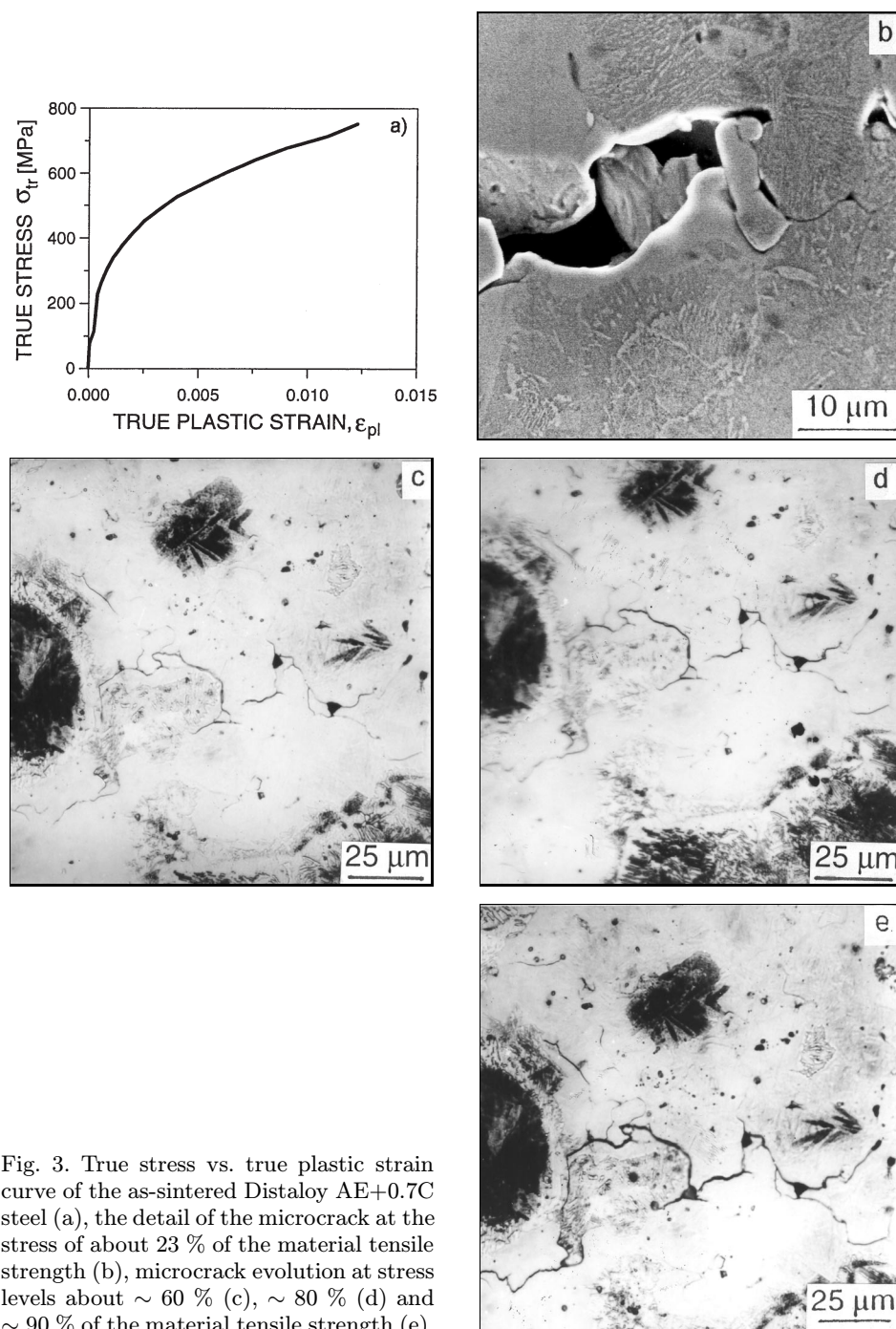


Fig. 3. True stress vs. true plastic strain curve of the as-sintered Distaloy AE+0.7C steel (a), the detail of the microcrack at the stress of about 23 % of the material tensile strength (b), microcrack evolution at stress levels about $\sim 60\%$ (c), $\sim 80\%$ (d) and $\sim 90\%$ of the material tensile strength (e).

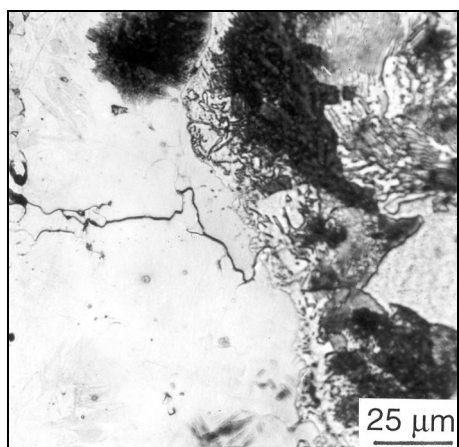


Fig. 4. Microcrack stopping at the interface boundary (as-sintered Distaloy AE+0.7C steel).

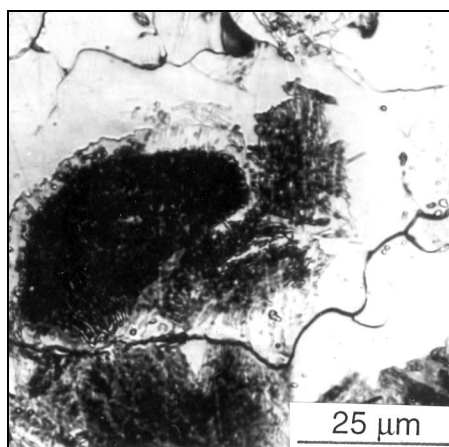


Fig. 5. Microcrack propagation along the interface boundary (as-sintered Distaloy AE+0.7C steel).

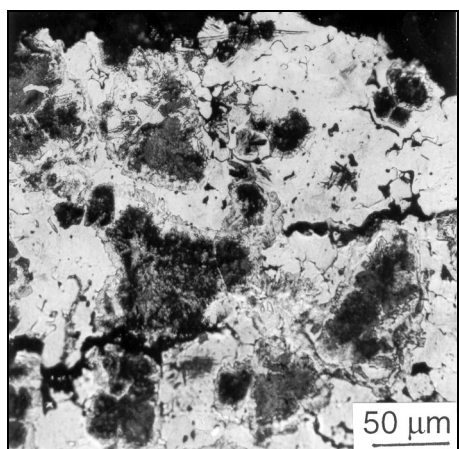


Fig. 6. Joining of the microcracks results in the formation of several large cracks and in development of a main crack.

dominantly from pore to pore (Fig. 7b, c). It can be assumed that their propagation is also controlled by the original particle surfaces. The microcracks in the heat-treated specimens seem to be shorter than those in the as-sintered specimens. The joining of individual microcracks occurs at tensile stresses about 80–90 % of the material tensile strength. The effect of pores situated at the original particle surfaces on the crack propagation is shown in Fig. 7d. Favourable distribution of high strength structural constituents in the heat-treated specimens results in the increase in the tensile strength from 603 MPa in the as-sintered state to 760 MPa in the heat-

treated material. Failure strain decreased from 1.2 % to 0.4 %.

The deformation behaviour of both as-sintered and heat-treated specimens is illustrated in Figs. 8a,b. The strain-hardening rate ($d\sigma_{tr}/d\varepsilon_{pl/tr}$) plotted as a function of the true plastic strain, ε_{pl} , is characterised by a high initial strain-

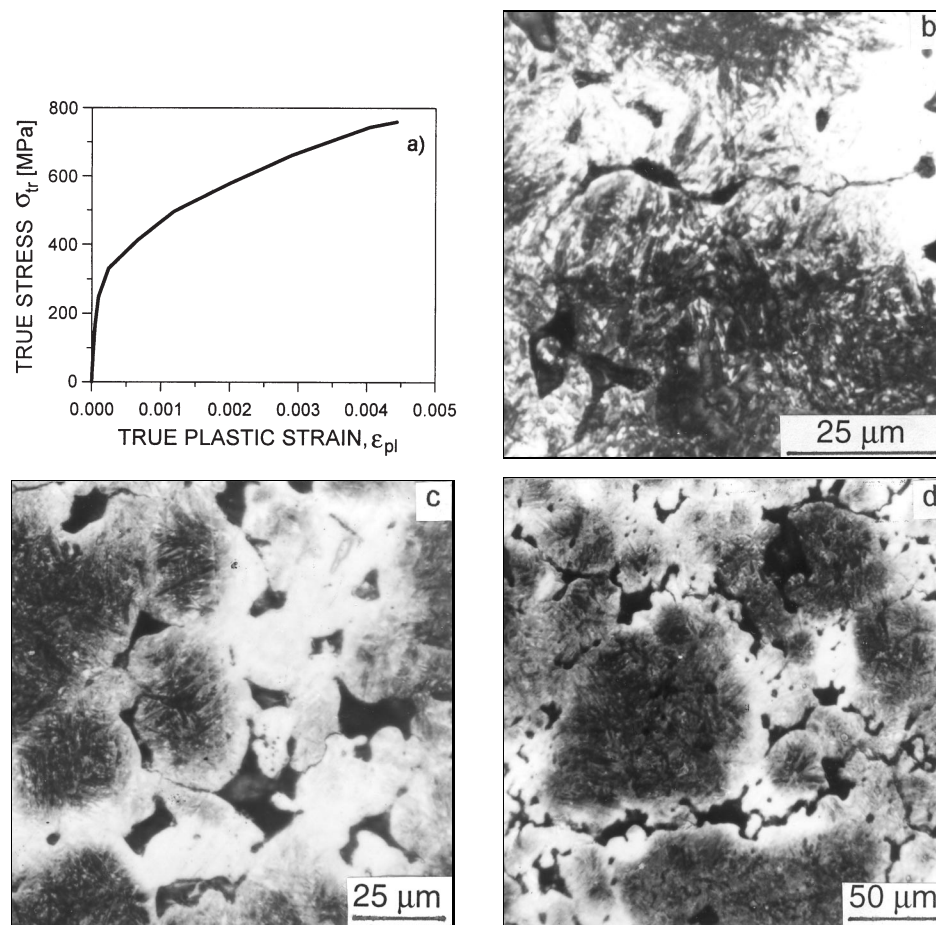


Fig. 7. The true stress vs. true plastic strain curve of the heat-treated Distaloy AE+0.7C steel (a), microcracks growth in the heat treated microstructure from pore to pore (b) and along the original particle surface (c), the effect of pores near the original particle surfaces on the crack propagation in the heat-treated material (d).

-hardening rate. It is connected with the primary plastic deformation of the most deformable regions (Ni-rich austenite). Note that in the heat-treated material, the high initial strain hardening rate region corresponds to a lower plastic strain than in the as-sintered material. During the further stress increase, the effect of the localised plastic flow is “absorbed” by the limiting effect of the surrounding hard microstructural constituents. The state of a high local stress concentration leads to the evolution of microcracks. Additional stress increase results in microcracks

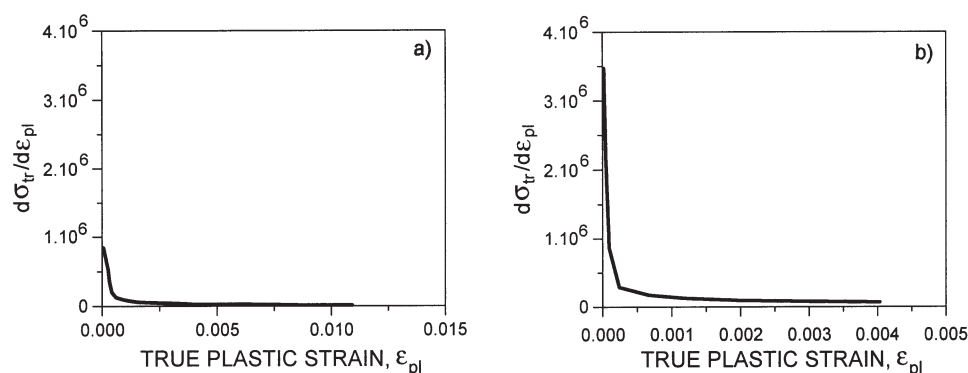


Fig. 8. The strain-hardening rate ($d\sigma_{tr}/d\varepsilon_{pl/tr}$) as a function of the true plastic strain ε_{pl} , for the as-sintered (a), and heat-treated Distaloy AE+0.7C (b).

growth through gradual joining to final fracture of the tested specimen. The presented results are in agreement with the results for failure evolution in Distaloy AE+0.5%C sintered specimens reported by Straffellini et al. [18].

4. Conclusions

Microcrack initiation and propagation processes in as-sintered and heat-treated Fe-Ni-Cu-Mo-C diffusion alloyed steel (Distaloy AE+0.7C) under tensile loading have been studied.

The microcrack initiation sites are dominantly connected with the pores situated in the martensitic regions in both as-sintered and heat-treated specimens. In the case of as-sintered microstructure, the microcrack propagation in martensitic areas occurs by mixed mechanisms involving intergranular failure, transgranular cleavage and separation on structural discontinuities. The branching and linking of microcrack path are controlled by the distribution of microstructural constituents. Increasing the tensile stress close to the material tensile strength results in a mutual microcracks joining. Several large cracks are formed and some of them result in the final fracture. In the heat-treated microstructure, the microcracks initiation is also connected with the pores situated in the martensitic regions localised near the original particle surfaces.

The tensile behaviour of both as-sintered and the heat-treated specimens is characterised by a high initial strain-hardening rate, which is connected with the plastic deformation development in the deformable microstructural regions during the first stages of loading.

The development of a microstructure with a higher resistance to the crack propagation via heat treatment can improve the strength of the Fe-Ni-Cu-Mo alloyed sintered steels.

Acknowledgements

The authors gratefully acknowledge the Scientific Grant Agency of Ministry of Education of the Slovak Republic and Slovak Academy of Sciences (Grant project No. 2/7228/20) and the Austria-Slovak Action (SAIA-Project No. 34s17) for the financial support of this work.

REFERENCES

- [1] EUDIER, M.: Powder Met., 5, 1962, p. 278.
- [2] ŠALAK, A.—MIŠKOVIČ, V.—DUDROVÁ, E.—RUDNAYOVÁ, E.: Powder Met. Int., 6, 1974, p. 128.
- [3] HAYNES, R.: Powder Met., 20, 1977, p. 17.
- [4] NAKAMURA, M.—TSUYA, K.: Powder Met., 22, 1979, p. 101.
- [5] FLECK, N. A.—SMITH, R. A.: Powder Met., 24, 1981, p. 121.
- [6] DANNINGER, H.—JANGG, G.—WEISS, B.—STICKLER, R.: Powder Met. Int., 25, 1993, p. 111.
- [7] DUDROVÁ, E.—PARILÁK, Ľ.—RUDNAYOVÁ, E.—PELIKÁN, K.: Powder Met. Int., 19, 1987, p. 23.
- [8] PELIKÁN, K.: Deformačné procesy a porušovanie pórovitého železa. [Kandidátska dizertačná práca]. Košice, Ústav materiálového výskumu SAV 1986.
- [9] MIURA, H.—BABA, T.—HONDA, T.: In: Advances in Powder Metallurgy & Particulate Materials. Compiled by Cadle, T. M., Narasimhan, K. S. Part 13. Princeton NJ, MPIF 1996, p. 42.
- [10] TREMBLAY, L.—CHAGNON, F.: In: Advances in Powder Metallurgy & Particulate Materials. Compiled by McKotch, R. A., Webb, R. Vol. 2. Part 13. Chicago, MPIF 1997, p. 53.
- [11] ŠLESÁR, M.—DUDROVÁ, E.—RUDNAYOVÁ, E.: Powder Met. Int., 24, 1992, p. 232.
- [12] PALMA, E. S.: In: Advances in Powder Metallurgy & Particulate Materials. Compiled by Cadle, T. M., Narasimhan, K. S. Part 7. Princeton NJ, MPIF 1996, p. 395.
- [13] POMPE, W.—LEITNER, G.—WETZIG, K.—GRABNER, W.: Powder Met., 27, 1984, p. 45.
- [14] MOON, J. R.: In: Proceedings of the International Conference Deformation and Fracture in Structural PM Materials. Eds.: Parilák, Ľ. et al. Vol. 1. Košice, IMR SAS 1996, p. 61.
- [15] STRAFFELINI, G.—FONTANARI, V.—MOLINARI, A.: In: Advances in Powder Metallurgy & Particulate Materials. Compiled by Lall, Ch., Neupaver, A. J. Part – Characterisation, Testing and Quality Control. Princeton NJ, MPIF 1994, p. 51.
- [16] CARABAJAR, S.—VERDU, C.—FOUGERES, R.: In: Advances in Powder Metallurgy & Particulate Materials. Compiled by Cadle, T. M., Narasimhan, K. S. Part 13. Princeton NJ, MPIF 1996, p. 201.
- [17] MOON, J. R.: In: Proceedings of the International Conference Deformation and Fracture in Structural PM Materials. Eds.: Parilák, Ľ. et al. Vol. 1. Košice, IMR SAS 1999, p. 214.

-
- [18] STRAFFELINI, G.—MOLINARI, A.—VISINTAINER, C.: In: Proceedings of 2000 Powder Metallurgy World Congress in Kyoto. Part 2. Eds.: Kosuge, K., Nagai, H. JSPPM, JPMA 2000, p. 1594.
- [19] HÖGANÄS Eisen – und Stahlpulver für Sinterformteile. Höganäs AB, Sweden 1998, p. 127.

Received: 2.8.2001